Impact of melting snow on the valley flow field and precipitation phase transition

Julie M. Thériault[a,*], Jason A. Milbrandt[b], Jonathan Doyle[a], Justin R. Minder[c], Gregory Thompson[d], Noemi Sarkadi[e], Istvan Geresdi[e]

[a] *Université du Québec à Montréal, Montréal, Québec, CANADA*
[b] *Atmospheric Numerical Prediction Research, Environment Canada, Dorval, Canada*
[c] *University at Albany, Albany, New York, US*
[d] *National Center for Atmospheric Research, Boulder, US*
[e] *University of Pécs, Faculty of Science, Szentagothai Research Center, Pécs, Hungary*

Abstract

The prediction of precipitation phase and intensity in complex terrain is challenging when the surface temperature is near 0°C. In calm weather conditions, melting snow often leads to a 0°C-isothermal layer. The temperature feedback from melting snow generates cold dense air moving downslope, hence altering the dynamics of the storm. A correlation has been commonly observed between the direction of the valley flow and the precipitation phase transition in complex terrain. This study examines the impact of temperature feedback from melting snow on the direction of the valley flow when the temperature is near 0°C. Semi-idealized two-dimensional simulations using the Weather Research and Forecasting model were conducted for a case of moderate precipitation in the Pacific Coast Ranges. The results demonstrate that the temperature feedbacks caused by melting snow affects the direction of the flow in valleys. Several microphysics schemes (1-moment bulk,

*Corresponding author
Email address: theriault.julie@uqam.ca (Julie M. Thériault)

2-moment bulk, and bin), which parameterize snow in different ways, all produced a valley flow reversal but at different rates. Experiments examining sensitivity to the initial prescribed snow mixing ratio aloft were conducted to study the threshold precipitation at which this change in the direction of the valley flow field can occur. All prescribed snow fields produced a change in the valley wind velocity but with different timings. Finally, the evolution of the rain-snow boundary with the different snowfields was also studied and compared with the evolution of the wind speed near the surface. It was found that the change in the direction of the valley flow occurs after the 0°C isotherm reaches the base of the mountain. Overall this study showed the importance to account for the latent heat exchange from melting snow. This weak temperature feedback can impact, in some specific weather conditions, the valley flow field in mountainous area.

Keywords: precipitation, complex terrain, rain-snow boundary, dynamic meteorology, microphysics

---

1. Introduction

Precipitation is one of the most important weather elements affecting our society. Its occurrence represents a crucial part of the global water cycle and it is a fundamental aspect of storms. The precipitation phase (i.e., rain versus snow) has a major impact on the water resources in the spring snowmelt season and plays an important role in determining flood hazard (e.g. Barnett et al., 2005; Elsner et al., 2010; White et al., 2002).

Formation and phase changes of precipitation are associated with diabatic heating and cooling of the environmental air due to latent heat exchanges.

Cooling due to melting snow can alter the temperature profile, which can in turn induce mesoscale circulations and influence the evolution of the storm. Lin and Stewart (1986) showed that melting-induced mesoscale circulation could extend as far as 50 km horizontally. Furthermore, in still weather conditions, the melting of snow often produces a deep isothermal layer of 0°C (Findeisen, 1940), which also leads to a change in precipitation from rain to snow.

These thermodynamic and dynamical feedbacks have been studied over complex terrain. Steiner et al. (2003) demonstrated through radar measurements that a change from up-valley to down-valley flow and a precipitation phase transition occur simultaneously. In particular, they observed that the top of the radar bright band correlated with the shear level where the flow direction changed. On the other hand, Zängl (2007) conducted numerical simulations of the same event and concluded that the melting process only has a small contribution to the change of the wind flow in the valley.

Similar radar patterns to those discussed in Steiner et al. (2003) were observed in other regions of the world. For instance, in the St-Lawrence River Valley, Quebec, Canada during The 1998 Ice Storm (Henson et al., 2011) as well as in the Whistler Area, British Columbia, Canada (Fig. 1) during the Vancouver 2010 Winter Olympics. In particular, a correlation between the change in precipitation phase, valley flow field, and a rapid decrease in surface temperature was observed on 13-14 February 2010 in the Whistler Area (Thériault et al., 2012) during the SNOW-V10 field project **(Isaac et al., 2014)**. It was hypothesized that the cooling from the melting snow was associated with the change in direction of the valley flow field.

The characterization of the rain-snow boundary in mountainous terrain has been addressed in several studies including Medina et al. (2005), Minder et al. (2011), Zängl (2007), Minder and Kingsmill (2013). In particular, Minder et al. (2011) performed numerical simulations to study the mesoscale features of the rain-snow boundary along mountainside. It was demonstrated that diabatic cooling by melting precipitation, adiabatic cooling from vertical motion, and microphysical timescales associated with melting all influenced the location of the rain-snow boundary along the mountainside, causing it to descend over a mountain windward slope. Their study also showed the predicted magnitude of the rain-snow boundary's descent varies substantially depending on microphysical parameterization.

The sensitivity to microphysical assumptions related to snow on the diabatic cooling effects and the resulting precipitation phase changes was examined in Milbrandt et al. (2014) in a simple one-dimensional framework for the 13-14 February 2010 case in the Whistler area. The snow quantity aloft corresponding to radar observations was prescribed with an observed temperature and humidity profile with melting and cooling rates simulated with a bulk microphysics scheme. It was shown that the cooling rate due to melting, and hence the resulting timing of the phase transition at the surface, can be quite sensitive aspects of the representation of snow in the model. This includes the assumed fall speed parameters, the number of prognostic moments, and constraints on the size distribution such as the lower limit of the slope parameter and the assumptions of the melting processes in schemes.

Given the difficulty of predicting the precipitation phase and intensity

when the temperature is near 0 °C, this study aims to better understand the impact of temperature feedbacks from melting snow on the direction of the valley flow field and on the precipitation phase. Semi-idealized two-dimensional simulations of the 13-14 February 2010 Whistler case were conducted using a mesoscale model in a systematic manner. First, the link between the temperature feedback from melting snow and the direction of the valley flow field is verified. A sensitivity experiment with various microphysical parameterization approach was also conducted. Second, the sensitivity to different precipitation rates, through prescribing different initial snowfields, is studied to investigate the threshold precipitation rates required to produce a change in the valley flow direction. Third, the evolution of the rain-snow line is compared to the rate of change of the valley flow for the different initial precipitation rates.

The paper is organized as follows. Section 2 describes the model configuration and experimental design. Section 3 summarizes the results from the control simulation along with the effects of suppressing diabatic cooling due to melting snow. The factor impacting the timing of the valley flow field are presented in section 4. The concluding remarks are given in Section 5.

2. Experimental design

2.1. Case overview

To test the impact of the temperature feedbacks from melting on the valley flow field and the precipitation phase transition, semi-idealized numerical simulations were performed based on the well-documented case of 13 February 2010 (Thériault et al., 2012). On this day, an intense warm-frontal

system slowly approached the British Columbia coastline as it elongated in a north-south orientation. This weather system was associated with heavy snow and a transition of precipitation from rain to snow along the mountainsides throughout most of the day. One particular geographic area and a multi-hour time period of this storm are used for this semi-idealized study.

This study focuses on the Callaghan Valley (VOD) located west of the base of Whistler Mountain (VOT) and south-west from the rawinsonde station (VOC) (Fig. 1) during the SNOW-V10 project (Isaac et al, 2014). A rapid decrease of the surface air temperature was observed in the Callaghan Valley (Fig. 2a) from 2230 UTC 13 February 2013 to 0000 UTC 14 February 2010. Soon after 0000 UTC, surface temperature reached 0°C and remained constant until 0600 UTC 14 February 2010. Figure 2b also shows that precipitation started in the valley (at VOT) when the air temperature began to drop. The fact that air temperature remained constant at 0°C for several hours strongly suggests that the temperature feedbacks from melting snow was a dominant forcing during that time period. Furthermore, the radar Doppler velocity (Fig. 3) in that region suggested a strong correlation between the rapid cooling of the surface air and the change in the direction of the valley flow. In particular, it showed a transition from up-valley flow prior to the onset of the rapid decrease in surface air temperature and to down-valley flow when the surface temperature reached 0°C (Fig. 3). The wind blows down valley flow the depth of the initial melting layer near the surface approximately 150 min after the onset of precipitation. The radar data used is discussed in (Joe et al., 2014).

2.2. Model setup

2.2.1. Model description

All of the simulations in this study were performed using the Weather Research and Forecasting (WRF) model, version 3.3.1 (Skamarock et al., 2008). The set-up involves a semi-idealized two-dimensional configuration, with modified orography corresponding to the Callaghan Valley area. The initial conditions and inflow lateral boundary conditions were based on observations of the case. The control run and the sensitivity tests with different prescribed precipitation rates (described below) were done using a two-moment bulk microphysics scheme as described in Milbrandt and Yau (2005b) (hereafter referred to as MY2). Given the sensitivity to the parameterization of snow shown in Milbrandt et al. (2014), it should be noted that the original version of the scheme has been used in this study.

The two-dimensional transect of interest is a vertical cross section oriented north-south passing through the radar location (VVO) and the Callaghan Valley (VOD) (Fig. 1b). The orography around the VOD station was centered in the domain; with 30 km of simplified orography, 60 km of flat terrain upwind (south of VOD), and 140 km downwind. The orography field is smoothed six times with a 1-2-6-2-1 filter and then interpolated to a 250 m grid spacing. The smoothing is necessary to remove numerical noise. For numerical stability at the time of model set-up, the elevation of the downwind side of the mountain was fabricated to continue the mountain topography. This prevents having an abrupt variation of the orography at the base of the mountain. The result is a near-bell shaped mountain (Fig. 4a) similar to that used in the default WRF idealized two-dimensional case.

The domain was chosen to be sufficiently large to minimize reflections from the lateral boundaries. Hence, the domain was set to 200 km with a 250 m grid spacing. The inflow and outflow boundaries were both set to open. To have a maximum number of vertical levels within the melting layer, 72 vertical grids have been used where the grid spacing varied from 20 m to 750 m for the z <9 km and 750 m for z >9 km. The top of the atmosphere is at 22 km. To minimize reflections from the lateral boundary, a 10 km damping layer was used at the top of the model to minimize the reflection of gravity waves from the upper boundary (Klemp et al., 2008). The simulation was integrated with time steps of 1 s for a total of 8 h. The Coriolis force and surface fluxes have been neglected in the simulations. All clouds and precipitation are represented by the microphysics scheme, which varies according to the experiment. No subgrid-scale condensation or convective schemes were used.

Note that the two-dimensional nature of our runs neglects the effects of the valley geometry on the thermodynamic and dynamic evolution of the valley atmosphere. For instance, in valleys with sloping side-walls a volume effect occurs that causes the valley to cool more rapidly by melting than a plain or a valley with vertical walls (e.g. Steinacker, 1983; Unterstrasser and Zängl, 2006). Thus by neglecting three-dimensional valley geometry we are likely underestimating the cooling rate of the valley air.

2.2.2. Initial conditions

The vertical temperature profile measured from VOC at 0000 UTC and 0600 UTC are shown in Fig. 5. At 0000 UTC, a shallow melting layer was present near the surface and 6 h later, that melting was replaced by a near

0°C-isothermal layer (Fig. 5b). Note that the wind direction also changed with time and elevation. For example, the flow changed from southerly wind to northerly wind between 0000 UTC 14 February 2010 and 0600 UTC 14 February 2010 at lower levels but stayed from the south at higher levels. The meteorological fields were initialized using the Whistler (VOC) sounding at 0000 UTC 14 February 2010 (Fig. 4 b-d). We assumed that the meteorological conditions were similar in the Callaghan Valley at the onset of precipitation. Note that the Callaghan Valley is located south-west of the Whistler sounding station (VOC) and that VOT observed the rapid cooling of air temperature 2 h later than in Callaghan valley. The observed meteorological fields were smoothed to prevent numerical instabilities. A comparison of the real and smoothed temperature, relative humidity and horizontal wind speed vertical fields are shown in Figs. 4b, c and d, respectively. To prevent snow sublimation aloft, the relative humidity has been increased to 95 % where the snow field is initialized (section 2.3). Finally, the north-south component of the wind speed was used.

For the control run, the MY2, which predicts the mixing ratio and total number concentration of 6 hydrometeor categories: clouds droplets, rain, pristine ice crystals, snow, graupel and hail, was used. From the precipitation sensor located at VOT, the precipitation rate was around 3 mm h^{-1} but the quantitative precipitation forecast (QPF) suggests that more precipitation occurred in the Callaghan Valley (VOD) (Thériault et al., 2012). We based our assumptions on QPF because no precipitation sensor was installed at VOD. Therefore, it was assumed that snow is falling continuously from above the melting layer to yield a surface precipitation rate of approximately

5 mm h^{-1}. The snow field was initialized with a mixing ratio, q_s = 1.25 g kg^{-1}, and total number concentration, N_s = 9860 m^{-3}, at the model level corresponding to an elevation of 2.3 km, based on observed radar reflectivity and temperature, assuming the relation between the snow intercept size distribution parameter and temperature from Thompson et al. (2004) (see Milbrandt et al. (2014) for details).

2.3. Sensitivity experiments

First, to show the impact of the temperature feedback from melting snow on the direction of the valley flow field, the control run was run while neglecting the temperature tendency due to melting snow. This sensitivity experiment has been repeated with another microphysical scheme, the Thompson et al. (2008) referred to as THOMP. Furthermore, we also repeated the control simulation with a bin microphysics scheme (e.g. Geresdi, 1998; Geresdi et al., 2014) referred as GERBIN. However the experiment neglecting the temperature feedback from melting was not performed due to the complexity of the scheme.

Second, the initial precipitation rates were varied to determine the sensitivity on the time at which the flow reversal/stagnation is reached. In weather forecasting in British Columbia, a rule of thumb is commonly used (Trevor Smith, personal communication Environment Canada, 2010) that a precipitation rate of 3 mm h^{-1} or more may lead to a valley flow reversal in complex terrain. The investigation of the precipitation rate thresholds associated with the change of direction of the valley flow is conducted for many initial snow mixing ratio, q_s = 2.5, 1.875, 1.25, 0.625, 0.3125 g kg^{-1}, corresponding approximately to resulting surface precipitation rates of 10,

7.5, 5, 2.5 and 1.25 mm h^{-1}, respectively. The initial wind speed will also affect the change in the direction of the valley flow field but only the initial precipitation rate has been studied. For each initial snow mixing ratio (or precipitation rate), the timing of the flow reversal at different stages was investigated by comparing the location of the 0°C-line on the mountainside as well as the location associated with mixed precipitation types (50% snow and 50% rain).

3. Impact of melting snow on the valley flow field

3.1. Control simulation

To ensure that the model reproduced acceptable atmospheric conditions we have studied the weather conditions at 60 min. This time was chosen because the 0 °C-isotherm is located approximately between VVO and VOD (Fig. 6). The top panel shows the vertical cross-section of the wind, temperature, and snow fields and the bottom panel the surface precipitation rates along the domain cross-section. First, the maximum simulated wind speed is in excess of 20 m s^{-1} above the barrier between 2 and 4.5 km. At this time, the wind at VVO remained in the up-valley direction but had started weakening with respect to the initial conditions. Second, the 0°-isotherm reached the ground approximately 5 km north of VVO on the mountainside. It has lowered by 400 m within 60 min in the simulations. Third, the snow field is initiated upstream of the barrier at altitude between 2.3-6 km with a mixing ratio value decreasing with height. The mixing ratio was chosen to yield a precipitation rate of 5 mm h^{-1} on the upstream side of the mountain. Snow is advected up to 50 km downstream of the barrier by the southerly

wind. Note that the rain and graupel fields aloft are not shown here because a specific attention is paid to the main atmospheric and precipitation fields occurring over the domain.

The surface precipitation rates along the cross-section show a mixture of rain and snow on the upstream side of the barrier (Fig. 6b). The precipitation changed to mainly snow with some graupel 5 km north of VVO, which corresponds to the location of where the 0 °C-isotherm reached the ground. Note that some graupel are produced by accretion with cloud droplets that formed due to ascending air along the mountainside. Graupel are also formed downwind, which is possibly caused by the updraft associated with gravity waves.

Now that we have an overall view of the weather conditions along the domain, the remaining analysis will focus on the horizontal distance in the vicinity of VVO and VOD (-10 km <y <15 km) and up to an altitude of 3 km above sea level.

3.2. Effects of melting on the valley flow field

To assess the impact of melting snow on the direction of the valley flow field, the temperature tendency due to the melting of snow was disabled in the microphysics scheme and the simulation was re-run and compared with the control run. A similar experiment was also conducted with the control setup but with the temperature tendency due to evaporation and sublimation suppressed. First, the impact of the processes are minor and were only present at the beginning (first 20 min) of the simulation until the atmosphere conditions are saturated. This was excepted since the atmosphere was so near to saturation with respect to liquid water.

The impact of the cooling associated with the melting of snow is clearly shown in Fig. 7. This illustrates the horizontal wind speed at two times of interest, which are 120 and 210 min, during the simulation. These times correspond to when the valley flow begins to change direction and when the down valley flow is distributed throughout the depth of the melting layer, respectively. The results are similar to the radar radial velocity fields at times corresponding to the onset of the change of the valley flow direction. For example, precipitation started at approximately 2230 UTC 13 February 2010 and the flow began to change direction 60 min later. Therefore, it took 90 min for the flow to change direction and fill the initial depth of the melting layer. The simulations suggest there is also 90 min time lapse between the start of the reversal and the moment when the valley flow field has entirely changed direction. This timing is comparable to the observed radar-inferred winds. Figure 7c and d show simulation results obtained when the diabatic cooling due to melting snow is turned off. The direction and strength of the valley flow remains constant throughout the simulation time. These results suggest that the temperature feedback associated with melting snow has an impact on the valley flow direction or stagnation.

Melting also affects the small-scale structure of the valley airflow. As melting begins, the associated cooling is not uniform with height. This localized cooling destabilizes the atmospheric profile (Findeisen, 1940). As a result, shallow convection temporarily occurs within and below the melting layer in our simulation. These can be seen in Fig. 8, which is discussed in the next section. Such melting-induced convection has been simulated previously using more idealized settings (e.g. Szyrmer and Zawadzki, 1999; Unterstrasser

and Zängl, 2006). While this has a notable but temporary effect on the valley flow structure, it appears that convective overturning has little overall effect on the rate at which the valley cools. This is consistent with the fact that the two-dimensional simulation results are similar, in terms of temperature changes and precipitation phase transition, to the one-dimensional results of Milbrandt et al. (2014), where convection is absent.

3.3. Mechanisms of the valley flow stagnation and reversal

The above analysis demonstrates the connection between melting and the valley flow, but what are the dynamical mechanisms whereby melting causes the flow to stagnate and reverse? In our simulations the effects of surface friction and Coriolis have been neglected. Thus, in a Lagrangian framework, horizontal pressure gradients are the only term capable of decelerating the horizontal momentum of an air parcel (baring substantial internal dissipation).

To analyze horizontal pressure gradients and their causes, Fig. 8 shows perturbation fields from the control experiment at t =120 and 240 min. Temperature and horizontal velocity are plotted as anomalies with respect to the initial profile. Pressure is plotted as an anomaly with respect to the $p(z)$ profile on the upwind boundary at the given time (to focus on instantaneous horizontal pressure gradients). All panels also show contours of equivalent potential temperature. These provide approximate streamlines where the flow is reversible moist-adiabatic. The vertical gradient also provides an approximate measure of the moist static stability. By $t = 120$ min, melting has nearly cooled all the air at the base of the mountain to 0°C, but at locations further upwind there is still a substantial layer of above-freezing air with the

remnants of melting-induced convection. Within the melting-cooled air is a zone of decelerated flow, centered at $x = 60$ km (Fig. 8a). A secondary zone of deceleration is found further up the mountain slope. A high-pressure anomaly of up to 0.5 Pa is found over the mountain slopes extending upwind (Fig. 8c). As flow along streamlines crosses isobars, air parcels increase their pressure and decelerate (Fig. 8d). Near $z = 1$ km streamlines rise over the layer of cooled and decelerated air just upwind of the base of the mountain.

At $t = 240$ min the flow configuration is similar, except the low-level high pressure anomaly and region of decelerated flow have expanded upwind past $x = 40$ km (Fig. 8g-h). This is coincident with a deepening of the layer of cooled air in the same region (Fig. 8e). Streamlines begin to rise far upwind of the mountain to surmount this layer.

When the temperature effect of melting is suppressed in the simulations, low-level cooling upwind is eliminated. A localized cool anomaly is still found above the windward slope (Fig. 9). A high-pressure anomaly is still found over the terrain, but it is confined to the upper portion of the windward slope. Flow deceleration is found near 1.5 km but stagnation and reversal do not occur. Near $z = 1$ km there is a localized acceleration of the flow associated with the lifting of an upwind near surface jet of faster flow.

What is the source of the horizontal variations in the low-level pressure anomaly that act to decelerate the flow and the differences between the simulations? One plausible hypothesis is that horizontal variations in snowfall rate above the melting layer lead to horizontal variations in melting-induced cooling that produce (by hydrostatic balance) horizontal pressure variations. Such horizontal variations in precipitation rate could be produced by oro-

graphic enhancement. However, Fig. 6 shows that the total precipitation rate is essentially uniform across the windward slope. Thus, while melting of orographically enhanced snowfall may sometimes enhance flow deceleration, such a mechanism does not explain the results of our experiment.

An alternative way to produce horizontal pressure gradients and decelerate the flow is through the lifting of stratified air. In a stratified atmosphere, local lifting over the windward slope of a mountain produces cold-temperature and high-density anomalies. If the atmosphere is hydrostatically balanced, these density anomalies directly result in high-pressure anomalies beneath them that can cause the low-level flow to decelerate, stagnate, or reverse (e.g. Smith, 1988, 1989). For uniform upwind conditions, simple terrain geometry, and in the absence of latent heating and Coriolis forcing the occurrence of low-level flow stagnation is controlled by the horizontal aspect ratio of the terrain and the non-dimensional mountain height: $H = Nh/U$, where N is the Brunt-Vaisalla frequency, U is the horizontal wind speed, and h is the height of the terrain (e.g. Pierrehumbert and Wyman, 1985; Smith, 1989; Smolarkiewicz and Rotunno, 1990). This parameter measures the nonlinearity of the flow and stagnation tends to occur above some threshold value of H that depends on the terrain shape. In scenarios such as the one we consider here, condensation of water vapor releases latent heat and modifies the flow dynamics, reducing windward pressure perturbations and flow deceleration. For flows of near-saturated air, the effects of condensation can be roughly accounted for in the above theory by replacing H with a moist non-dimensional mountain height $H_m = N_m h/U$ (e.g. Jiang, 2003) where N_m is a moist version of the Brunt-Vaisalla frequency (Durran and Klemp,

1982).

The interaction of the above mechanism with melting can be understood by considering the evolution of the lowest 1 km of the atmospheric profile upwind of the terrain (Fig. 10). Initially the low-level flow is unsaturated. The profile is stable with respect to dry lifting, as evidenced by the profile of θ (Fig. 10 d). Although N_m^2 is initially slightly negative below $z = 1$ km (Fig. 10 f), since the flow is unsaturated, the profile is actually moist stable, evidenced by the constant θ_e in the lowest 0.4 km. As the simulation progresses, snow falls into the lowest layers and melts (Fig. 10 b). This gradually cools the air below 1 km to 0°C (Fig. 10 a). The cooling brings this layer to saturation and excess water vapor is condensed out (Fig. 10 c). This isothermal layer increases the dry stratification as represented by θ and the moist stratification as represented by θ_e and N_m (Fig. 10 d-f). When the temperature effect from melting is suppressed, only very modest amounts of moistening and cooling occur in the lowest few hundred meters due to sublimation (Fig. 10 g-i). These changes only cause slight modifications to the upwind stratification (Fig. 10 j-l).

To explore changes in the dynamical regime associated with the observed changes in the upwind profile, values of H_m are calculated before and after melting. These are computed by averaging the horizontal winds and N_m of the upwind profile from the surface to 2 km, and setting h=1.2 km. Before melting $H_m = 1.9$. Although this is above the typical threshold of about H=0.85 for flow stagnation for a two-dimensional ridge (e.g. Huppert and Miles, 1969), our results are not directly comparable with previous studies due to the non-uniform vertical profile. More importantly, the excess N_m

produced by melting increases H_m to 3.3, indicating that melting has changed the upwind profile in such a way that flow stagnation is much more favored. In the no-temperature effect from melting snow experiment sublimation H_m only increases to 2.2, a much more modest change.

When the temperature effect of melting is suppressed, the lack of a substantial pressure perturbation upwind of about $x = 65$ km is due to the minimal lifting upwind of this region and lack of stratification below $z = 1$ km (Fig. 9 c and f). In this experiment the lifting-induced pressure anomaly causes deceleration that is focused above 1.2 km (Fig. 9 g and h). When melting is included the air below z =1 km becomes much more strongly stratified (Fig. 8). Lifting of this melting-cooled air near the base of the mountain produces a pressure perturbation, which produces much more substantial flow deceleration (Fig. 8 c-d and g-h). As air upwind lifts over the decelerated air, pressure anomalies are produced upwind of the foot of the terrain (Fig. 8 c and g). As found in previous studies (e.g. Pierrehumbert and Wyman, 1985) the region of decelerated flow propagates far upwind of the mountain. In this and other two-dimensional simulations without Coriolis forcing the upwind propagation continues indefinitely (Pierrehumbert and Wyman, 1985). Eventually, the windward deceleration proceeds to the point where the windward flow stagnates and reverses (Fig. 8 h).

In summary, melting modifies the windward flow dynamics primarily via its effects on the upwind atmospheric profile. By stratifying the low-level air, melting moves the flow into a dynamical regime with high H_m where low-level pressure perturbations produced by lifting are able to decelerate the flow to the point of stagnation and reversal.

4. Factors impacting the timing of the valley flow field

4.1. Cloud and precipitation microphysics parameterization approach

To examine the sensitivity to different parameterizations of snow, the same experiments were run using two other microphysics schemes. They are the THOMP bulk scheme, which has some notable differences in treatment of snow compared to MY2, and the bin-resolving scheme (GERBIN).

Each microphysics scheme used in this study (MY2, THOMP and GERBIN) is constructed differently but considers the same microphysical processes for melting snow. These processes are (1) equilibrium between melting rate of snow, condensational heating and diffusion of sensible heat by conduction; (2) mass conversion from accretion and collection of cloud droplets and rain drops in the melting layer. However, the behavior of each scheme in this intercomparison is different because of specific basic assumptions such as initial size distribution, number of moments predicted and characteristics of categories. For example, the amount of mass converted into rain depends on the atmospheric conditions (wet bulb temperature) but this equation is integrated over an analytic size distribution (for the bulk microphysics scheme). Therefore, even if the atmospheric conditions are the same, the amount of mass melted into rain depends on the parameters of the size distribution (N_0 and λ) assumed. In the case of a bin microphysics scheme, the evolution of the precipitation characteristics is highly detailed and considered to be more realistic because there is discrete number of mass bins of snow. This allows for a more accurate representation of the melting rate throughout the size distribution of melting snow (Geresdi et al., 2014). Furthermore, the treatment of melted water is different between bulk and bin scheme approaches.

For instance, in the bin schemes no shedding occur as opposed to bulk scheme where the melted water immediately sheds off the snowflakes. This difference affects the number and the mean size of rain drops produced by the melting process.

As shown in Figure 11, all microphysics schemes produced valley flow stagnation in the control case. On the other hand, when the temperature tendency from melting snow was shut off, none of the schemes produced a change in the valley flow direction. We were able to disable the temperature feedbacks from melting snow in the bulk scheme only due to the complexity of the parameterization in a bin-resolving approach. Wind speed starts to decrease 20 min after temperature starts to decrease, finally reaching 0 m s^{-1} at 180 min, 210 min and 200 min for the MY2, THOMP and GERBIN, respectively. The wind speed and temperature remain nearly constant throughout the time evolution when the cooling rate from melting snow is turned off (MY2 and THOMP only). For a precipitation rate of 5 mm h^{-1}, the wind speed decreases to 0 m s^{-1} 2.5 to 3 h after the surface temperature started to decrease depending on the microphysics scheme used.

In terms of the surface temperature evolution, as expected, all microphysics parameterizations show a cooling when the temperature feedback from melting is considered. The temperature starts to decrease at the surface after 20 min in the simulation. This initial decrease in temperature early in the simulations is likely due to evaporation and sublimation, as the atmosphere is not yet saturated with respect to liquid water. The cooling is mainly due to the temperature feedback from the melting of snow because it eventually reaches a constant value of 0°C at 100 min for the MY2 scheme

and 130 min for the THOMP and 110 for the GERBIN schemes. The timing of the cooling rates is faster for the MY2 scheme because snow is assumed to fall faster than in THOMP and GERBIN schemes. However, when snow falls in the melting layer, its terminal velocity is doubled when falling at temperature above 0 °C in THOMP whereas it remains the same in MY2. In that case, the residence time of snow in the melting layer is reduced which decreases the melting rate and therefore the temperature feedback from melting snow. Furthermore, the difference between the bin-resolving approach and the bulk are the assumptions associated with the ice category transferred to liquid water category. While the bulk schemes continuously produce water drops by shedding snow and graupel, the bin approach forms water drops at low concentration and of relatively larger size throughout the melting process (Geresdi et al., 2014). In GERBIN the melted snowflakes are transferred to the water drop category if the fraction of the melted water is larger than 0.85. Note that when the temperature is near 0°C even the smaller snowflakes do not melt completely, which is not the case in the bulk approach.

This impact on the temperature evolution directly affects the types of precipitation reaching the surface. As expected, when the temperature feedback from the melting snow is neglected, the temperature and wind speed do not vary significantly so a mixture of rain and snow is produced at VVO with 5 times more wet snow compared to rain. Only the MY2 scheme produced graupel at the surface. This could be due to the decrease in the strength of the vertical motion over the barrier, and in turn in the amount of available cloud water to enable snow conversion to graupel. Also, the treatment of snow conversion to graupel are different in THOMP and MY2 as MY2 tends

to generally produce more graupels than THOMP. For the case where full microphysics is considered, a transition from rain to snow is produced at the base of the mountain in addition to a trace of graupel between 60 to 150 min. Note that the rate of transition from snow to rain is similar. For instance, the time at which the precipitation type at the surface is half rain and snow occurs between 68 and 80 min for all schemes. The differences are caused by the different parameterization of snow and by the different treatment of shedding in the three approaches tested.

4.2. Prescribed snow field aloft

The time evolution of the direction of the valley flow field and the timing of the 0°C line traveling along the mountainside have been studied by varying the initial precipitation rate prescribed. This has been conducted only with the MY2 microphysics scheme. These sensitivity experiments allow us to address the following questions: (1) Is there a minimum precipitation rates that would cause reversal or stagnation of the valley flow field? (2) What is the relative timing of the 0°C-line descending the mountainside and the complete reversal of the valley flow?

The change in the valley flow direction with full microphysics has been studied for 6 prescribed precipitation rates. The times at which the valley flow field starts to change direction and when the valley flow has completely changed direction (<1 km ASL) have been calculated and are shown in Fig. 12a. The time at which the valley flow starts changing direction is defined by the time at which the wind speed becomes negative below the 0°C-isotherm and between VVO and VOD. On the other hand, the timing associated with completely reversed valley flow (<1 km ASL) was obtained based on the

maximum number of model grid points between VVO and VOD associated with a negative wind speed.

First, the onset of the change in the wind direction occurs near the top of the melting layer where cooling due to melting snow is present. As snow continues to fall towards the surface, the change in the flow direction starts to propagate downward. Second, all prescribed precipitation rates lead to a change in the direction of the valley flow field but at different timings (Fig. 12a). Finally, the onset of direction change varies by 40 min from 1.25 mm h^{-1} to 5 mm h^{-1} and this event occurs much faster for precipitation rates >5 mm h^{-1}. In particular, a precipitation of 10 mm h^{-1} has to be sustained for nearly 2 h to start changing the direction of the valley wind whereas it would take 4 h for a precipitation rate of 1.25 mm h^{-1}.

Because of all the other processes influencing the temperature evolution along the mountainside such as adiabatic cooling/warming, the complete reversal of the flow occurred before the 0°C-line reached the base of the mountain. It takes nearly 360 min for the valley flow to completely change direction at a precipitation rate of 1.25 mm h^{-1} and 180 min at 10 mm h^{-1}. Finally, the elapsed time between the onset of direction change and the completion of the reversal increases with increasing precipitation rate. For example, this time span is 65 min at 10 mm h^{-1} and 110 min at 1.25 mm h^{-1}.

Figure 12b plots the time when the 0°C-line and the 50/50 rain/snow line have, respectively, descended the mountainside under different precipitation rates. As the precipitation rate increases, the time for the 0°C-line to descend the mountainside varied from 480 min for a 1.25 mm h^{-1} to 90 min for 10

mm h^{-1}. The time for the 50/50 rain/snow line is shorter because that line is located at lower elevation than the 0°C-line. As expected, the time needed for these lines to reach the base of the mountain is faster for higher precipitation rate (10 mm h^{-1}) than for lower ones (1.25 mm h^{-1}). This is due to the fact that low precipitation rate is associated with less mass melting into snow and cooling off the top of the melting layer. Notice that the timing of change in the flow direction and the timing of rain-snow boundary descending the mountainside vary similarly.

The time associated with the change in the valley flow direction throughout the depth of the valley generally occurs after the 0°C reached the base of the mountain (Fig. 13). For example, the valley flow change direction ∼100 min after the 0°C-line has reached the base of the mountain (VVO) for a precipitation rate of 5 mm h^{-1}. In this case, the onset of reversal and the arrival of the 0 °C-line at the base of the mountain occur simultaneously. On the other hand, the flow starts to reverse just when the 0°C-line is still going down the valley for a precipitation rate of 1.25 mm h^{-1}. For the lowest precipitation rate, the cooling rate is slower hence decreasing the lag time between the cooling from melting snow and the change in the valley flow direction.

5. Summary and conclusion

This study investigated the impact of the temperature feedback from melting snow on the low-level flow field and precipitation phase transition in complex terrain. In particular, experiments examining the temperature feedbacks on the direction of the valley flow and the evolution of the rain-snow

line have been conducted. To address these issues, numerical simulations using a semi-idealized setup have been used. The WRF model was initialized with the vertical temperature, humidity and wind speed measured at VOC. Snow was allowed to fall continuously from aloft at a constant rate on the upstream side of the mountain, with no synoptic forcing.

A series of sensitivity experiments were conducted and the results showed that the simulations with all of the microphysics schemes tested reproduced a change in the valley flow field direction when the diabatic effect of melting snow is considered. Although all schemes produced a slightly different timing.

Further sensitivity studies with different precipitation rates led to the following conclusions:

- The timing of the flow reversal as well as the depth of the layer in which it was produced was comparable to the radar data for the control simulation.

- All precipitation rates tested produced a flow reversal/stagnation but at different rates. However, the time to produce it is much longer for lower precipitation rates. That means that calm synoptic conditions need to be present of up to 8 h to observe a flow reversal produced by a 1 mm h^{-1} snowfall rate. Since upwind evolution is key, adjusting snow rate can only affect the timing of reversal, not its existence. Even very light snowfall will eventually cool and stratify the air, leading to reversal. However, in reality, only weak long lasting synoptic conditions could lead to change in the flow direction in the valley.

- The speed of the rain-snow boundary traveling down the mountain

increases linearly with increasing the time for the valley flow to change direction as the initial precipitation rate increases. It generally reaches the base of the mountain before the flow reversal has completely fill up the initial depth of the melting layer.

Further study should be conducted to verify the results with a full atmospheric model. It would be useful to study the impact of three-dimensional valley geometry and the surrounding mountains on the timing of the flow reversal. Also, an idealized study could be conducted to examine the relative timing of large-scale warm air advection and cooling due to melting of snow. For instance, given a synoptic forcing and a snowfall rate, one could determine if the flow will reverse or not.

Overall, this study showed the importance that microphysical processes can have on mesoscale flow and the conditions at the surface. This was exemplified by the challenging prediction of local weather conditions during the Vancouver 2010 Winter Olympics which was critical for safe and fair competition.

Acknowledgments

We would like to thank the Natural Sciences and Engineering Research Council of Canada (NSERC) and the Fond Quebecois de la recherche sur la nature et les technologies (FRQNT) for the financial support needed to accomplish this work. The research made by N. Sarkadi and I. Geresdi was supported by Hungarian Scientific Research Found (number: 109679). We would like to acknowledge the contribution to constructive discussion with participants, in particular Roy Rasmussen, at the 8th International Cloud Modeling Work-

shop held in Warsaw, Poland in July 2012. The authors would like to acknowledge the SNOW-V10 principal and co-investigators for sharing the data used in this study.

6. References

Barnett, T. P., Adam, J. C., Lettenmaier, D. P., 2005. Potential impacts of a warming climate on water availability in snow-dominated regions. Nature 438, 303–309.

Durran, D. R., Klemp, J. B., 1982. On the effects of moisture on the brunt-v aisa l a frequency. J. Atmos. Sci. 39 (10), 2152–2158.

Elsner, M., Cuo, L., Voisin, N., Deems, J., Hamlet, A., Vano, J., Mickelson, K., Lee, S.-Y., Lettenmaier, D. P., 2010. Implications of 21st century climate change for the hydrology of Washington State. Climatic Change 102 (1-2), 225–260.

Findeisen, C., 1940. The formation of the 0°C isothermal layer and fractocumulus under nimbostratus. Meteorol. Z. 54, 49–54.

Geresdi, I., 1998. Idealized simulation of the colorado hail storm case: comparison of bulk and detailed microphysics. Atmospheric Research 45, 237–252.

Geresdi, I., Sarkadi, N., Thompson, G., 2014. Effect of the accretion by water drops on the melting of snow flakes. Atmospheric Research, in press.

624 Henson, W., Stewart, R., Kochtubajda, B., Thériault, J., Sep. 2011.
625 The 1998 Ice Storm: Local flow fields and linkages to precipitation.
626 Atmospheric Research 101 (4), 852–862.
627 URL http://linkinghub.elsevier.com/retrieve/pii/S0169809511001645

628 Huppert, H., Miles, J., 1969. Lee waves in a stratified flow. Part 3: Semi-
629 elliptical obstacle. Journal of Fluid Mechanics 35 (3), 481–496.

630 Isaac, G. A., Joe, P., Mailhot, J., Bailey, M., Bélair, S., Boudala, F., Brug-
631 man, M., Campos, E., Carpenter, R., Crawford, R. W., Cober, S., Denis,
632 B., Doyle, C., Reeves, H., Gultepe, I., Haiden, T., Heckman, I., Huang, L.,
633 Milbrandt, J., Mo, R., Rasmussen, R., Smith, T., Stewart, R. E., Wang,
634 D., 2014. Science of Nowcasting Olympic Weather for Vancouver 2010
635 (SNOW-V10): A World Weather Research Programme project. SNOW-
636 V10 Special Issue Pure and Appl. Geophys. 171, 1–24.

637 Jiang, Q., 2003. Moist dynamics and orographic precipitation. Tellus Series
638 A-dynamic Meteorology and Oceanography 55 (4), 301–316.

639 Joe, P., Scott, B., Doyle, C., Isaac, G. A., Cober, S., Mirecki, F., Gultepe,
640 I., Campos, E., Donaldson, N., Hudak, D., Stewart, R. E., 2014. The
641 monitoring network of the Vancouver 2010 Olympics. SNOW-V10 Special
642 Issue Pure and Appl. Geophys. 171, 25–58.

643 Klemp, J. B., Dudhia, J., Hassiotis, A. D., 2008. An upper gravity-wave
644 absorbing layer for nwp applications. Monthly Weather Review 136, 3987–
645 4004.

Lin, C. A., Stewart, R. E., 1986. Mesoscale circulations initiated by melting snow. J. Geophys. Res. 91, 13299–13302.

Medina, S., Smull, B. F., R. A. Houze, M. S., 2005. Cross-barrier flow during orographic precipitation events: Results from MAP and IMPROVE. J. Atmos. Sci. 62.

Milbrandt, J., Thériault, J., Mo, R., 2014. Modeling the phase transition associated with melting snow in a 1d kinematic framework: Sensitivity to the microphysics. Pure and Applied Geophysics 171 (1-2), 303–322.

Milbrandt, J. A., Yau, M. K., 2005b. A multi-moment bulk microphysics parameterization. Part II: A proposed three-moment closure and scheme description. J. Atmos. Sci. 62, 3065–3081.

Minder, J. R., Durran, D. R., Roe, G. H., 2011. Mesoscale controls on the mountainside snow line. J. Atmos. Sci. 68, 2107–2127.

Minder, J. R., Kingsmill, D. E., 2014/09/19 2013. Mesoscale variations of the atmospheric snow line over the Northern Sierra Nevada: Multiyear statistics, case study, and mechanisms. Journal of the Atmospheric Sciences 70 (3), 916–938.

Pierrehumbert, R. T., Wyman, B., 1985. Upstream effects of mesoscale mountains. J. Atmos. Sci. 42 (10), 977–1003.

Skamarock, W., Klemp, J., Dudhia, J., Gill, D., Barker, D., Duda, M., Huang, X.-Y., Powers, J., 2008. A description of the advanced research wrf version 3. Tech. rep., NCAR Techn. Note NCAR/TN-475+STR, 113 pp.

669 Smith, R., 1988. Linear theory of stratified flow past an isolated mountain
670 in isosteric coordinates. J. Atmos. Sci. 45, 3889–3896.

671 Smith, R., 1989. Mountain-induced stagnation points in hydrostatic flow.
672 Tellus 41a, 270–274.

673 Smolarkiewicz, P. K., Rotunno, R., 1990. Low froude-number flow past 3-
674 dimensional obstacles .2. upwind flow reversal zone. J. Atmos. Sci. 47 (12),
675 1498–1511.

676 Steinacker, R., 1983. Diagnose und prognose der schneefallgrenze (diagnosing
677 and predicting the snowline). Wetter Leven 35, 81–90.

678 Steiner, M., O. Bousquet, R. A. H., Smull, B. F., Mancini, M., 2003. Air-
679 flow within major alpine river valleys under heavy rainfall. Quart. J. Roy.
680 Meteor. Soc. 129, 411–431.

681 Szyrmer, W., Zawadzki, I., 1999. Modeling of the melting layer. Part I: dy-
682 namics and microphysics. J. Atmos. Sci. 56, 3573–3592.

683 Thériault, J. M., Rasmussen, R., Smith, T., Mo, R., Milbrandt, J. A., Brug-
684 man, M. M., Joe, P., Isaac, G. A., Mailhot, J., Denis, B., 2012. A case
685 study of processes impacting precipitation phase and intensity during the
686 vancouver 2010 winter olympics. Wea. Forecasting 27 (6), 1301–1325.

687 Thompson, G., Field, P. R., Rasmussen, R. M., Hall, W. D., 2008. Ex-
688 plicit forecasts of winter precipitation using an improved bulk microphysics
689 scheme. Part II: Implementation of a new snow parameterization. Monthly
690 Weather Review 136 (12), 5095–5115.

691 Thompson, G., Rasmussen, R. M., Manning, K., 2004. Explicit forecasts of
692 winter precipitation using an improved bulk microphysics shceme. Part I:
693 Description and sensitivity analysis. Mon. Wea. Rev. 132, 519–542.

694 Unterstrasser, S., Zängl, G., 2006. Cooling by melting precipitation in alpine
695 valleys: An idealized numerical modelling study. Quarterly Journal of the
696 Royal Meteorological Society 132 (168), 1489–1508.

697 White, A. B., Gottas, D. J., Strem, E. T., Ralph, F. M., Neiman, P. J., 2002.
698 An automated brightband height detection algorithm for use with doppler
699 radar spectral moments. Journal of Atmospheric and Oceanic Technology
700 19, 687–697.

701 Zängl, G., 2007. Reversed flow in the south-alpine Toce valley during MAP-
702 IOP 8: Further analysis of latent cooling effects. Q. J. R. Meteorol. Soc.
703 133, 1717–1729.

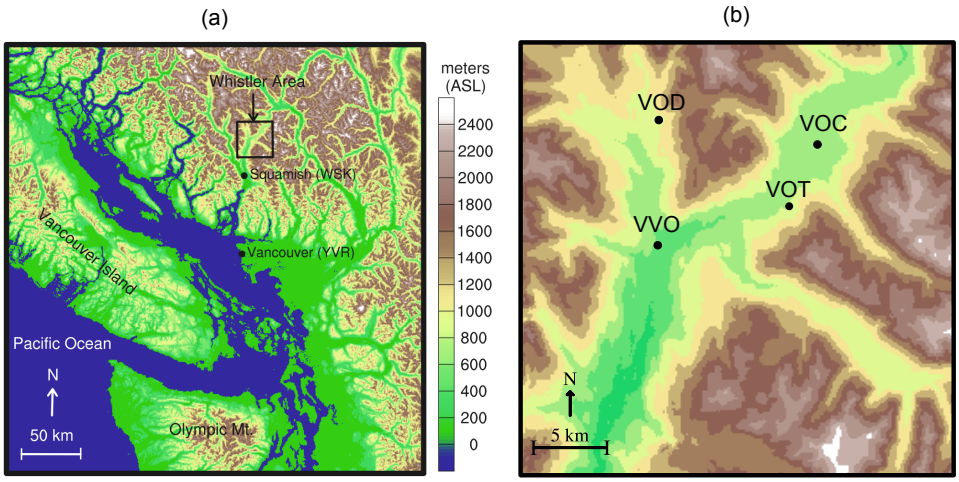

Figure 1: (a) Western North America and (b) the Whistler area British Columbia. The Callaghan Valley is located at VOD, the radar was located at VVO and the soundings were launched from VOC. The precipitation rate shown in Fig. 2b was measured at VOT because no precipitation sensors were installed in the Callaghan Valley. Figure adapted from Thériault et al. (2012).

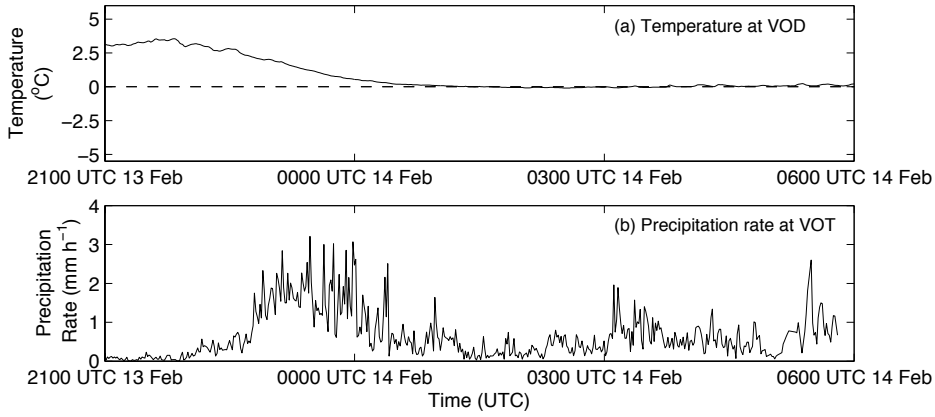

Figure 2: (a) The surface temperature evolution at VOD in the Callaghan Valley shows a rapid decrease in temperature. (b) The precipitation rate measured by FD12P at VOT, which is the base of Whistler Mountain. The onset of precipitation in the Whistler Area was at 2230 UTC. The figure is adapted from Thériault et al. (2012).

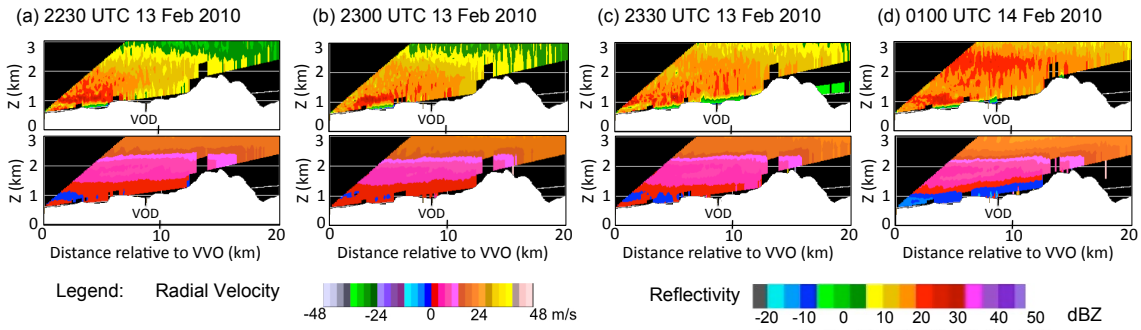

Figure 3: The radar range-height indicator (RHI) of radar reflectivity (top panels) and radial doppler velocity (bottom panels). (a) is before precipitation started (b) is 30 min after the onset of precipitation (c) is when the valley flow starts to reverse and (d) is when the valley flow has completely change direction. This is a north-south cross-section looking northward from VVO into the Callaghan Valley.

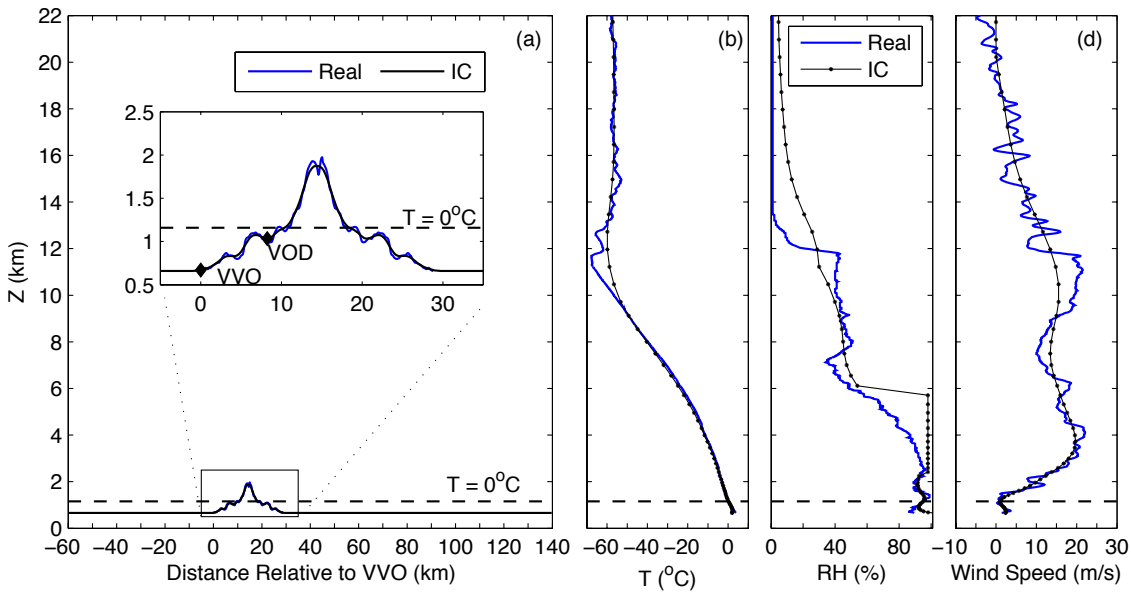

Figure 4: An overview of the experimental design. (a) is the domain chosen and the real (blue) and smoother (black) topography. (b)-(d) are the observations measured by the sounding launched from VOC at 0000 UTC 14 February 2010 (fig 5a). (b) is the temperature, (c) is the relative humidity and (d) is the wind speed. The blue lines are the observed value and black are the WRF initial conditions.

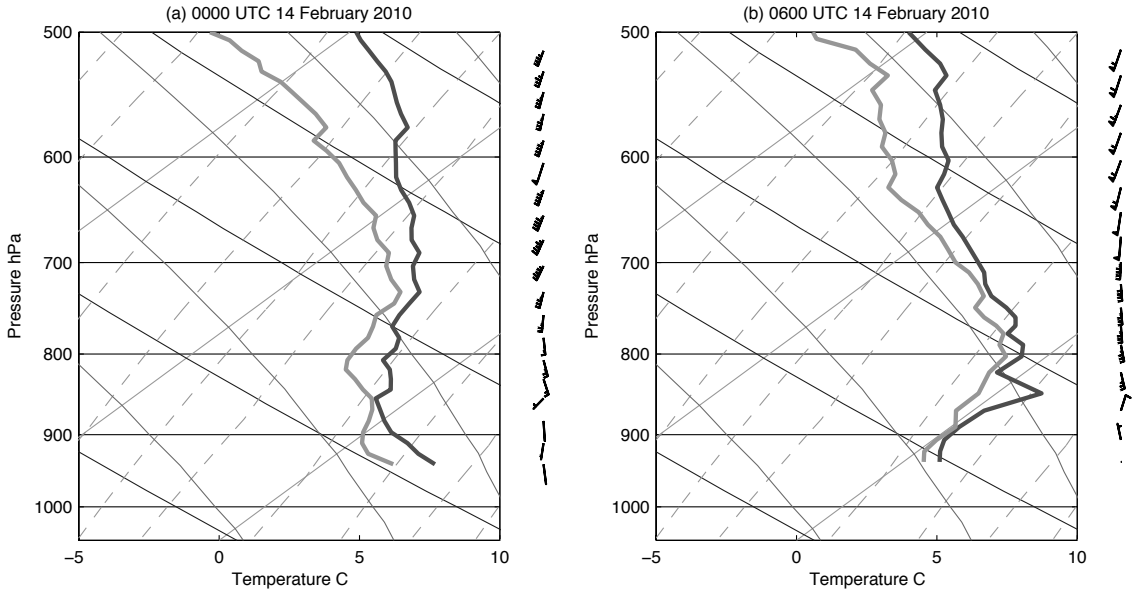

Figure 5: The skew-T from Whistler area (VOC) at (a) 0000 UTC 14 February 2010 and at (b) 0600 14 February 2010.

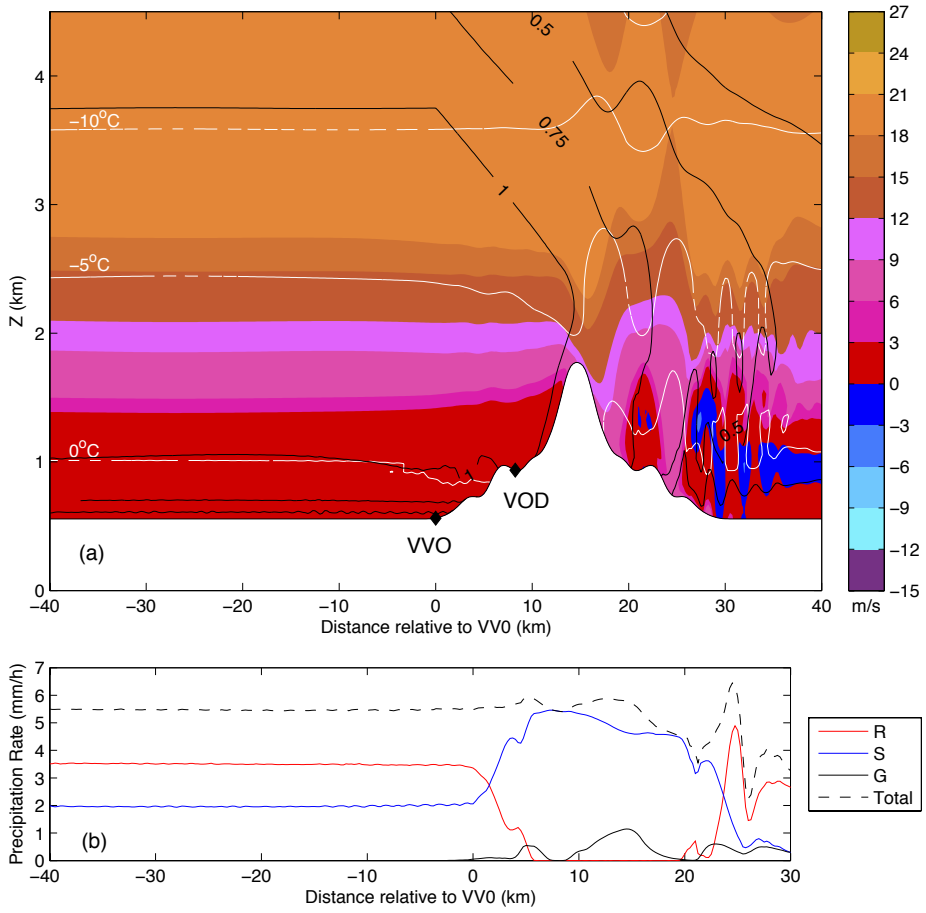

Figure 6: Atmospheric conditions associated with the control run at 60 min. (a) The horizontal wind speed (filled contour), the temperature (white lines) and mass mixing ratio of snow (g kg^{-1}) (black lines) fields across the full horizontal domain but only up to 8 km above sea level. (b) The precipitation rate of snow, rain and graupel at the surface across the same domain.

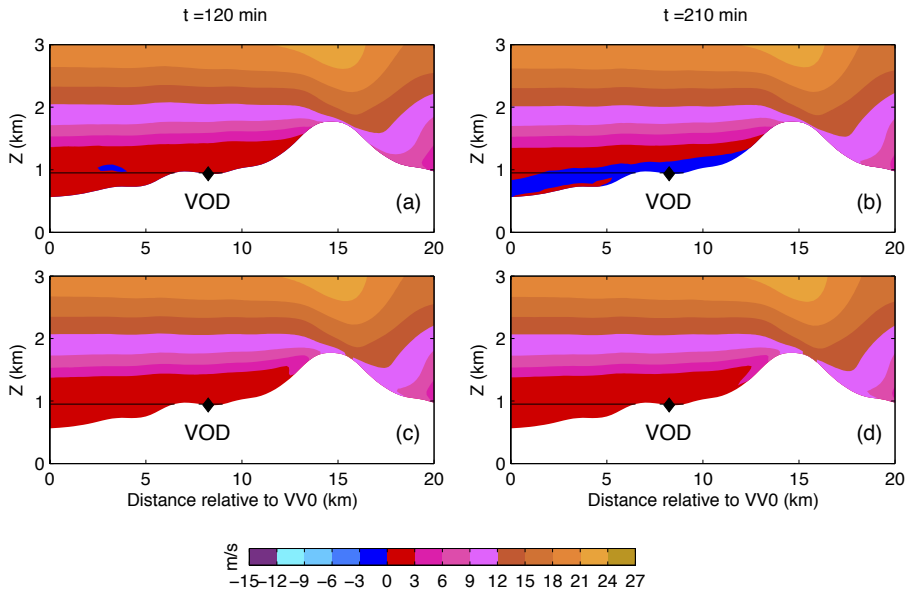

Figure 7: The horizontal wind speed using the same color bar as the radar radial velocity to allow direct comparison. This is a sub-domain of Fig. 6 of comparable size to the radar image (Fig. 3) to facilitate the comparison of the fields. The top panels (a and b) are the control run, which includes all microphysical processes. The bottom panels (c and d) include the experiment suppressing the effect of cooling due to melting snow. The radar is located at VVO at 0 km horizontal distance. The black line indicates the initial 0 °C line. The left panels are the time associated with a change in the valley flow direction and the right panels are the time when the valley flow field has completely change direction.

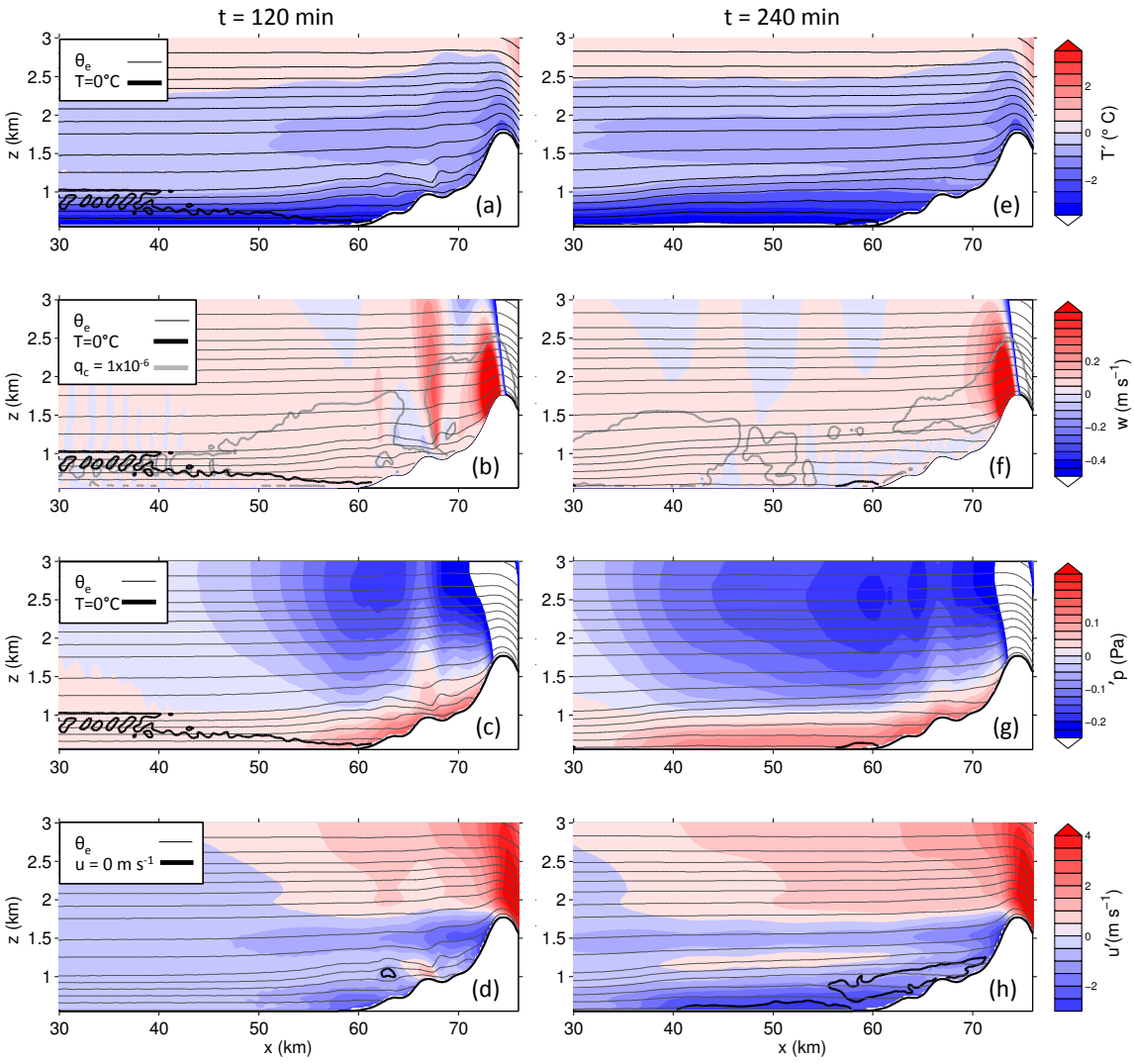

Figure 8: Vertical sections showing perturbation fields from the control experiment. (a)-(d) show results at t = 120min. (e)-(h) show results at t=240min. (a) and (e) show temperature perturbations with respect to the initial $T(z, t_0)$ profile. (b) and (f) show vertical velocity. (c) and (g) show pressure perturbations with respect to the current upwind profile $p(z, t, x_o)$. (d) and (h) show velocity perturbations with respect to the initial $u(z, t_0)$ profile and a bold contour denotes regions of flow reversal. All panels include thin contours of θ_e. (a)-(c) and (e)-(g) include a bold contour denoting the 0°C isotherm.

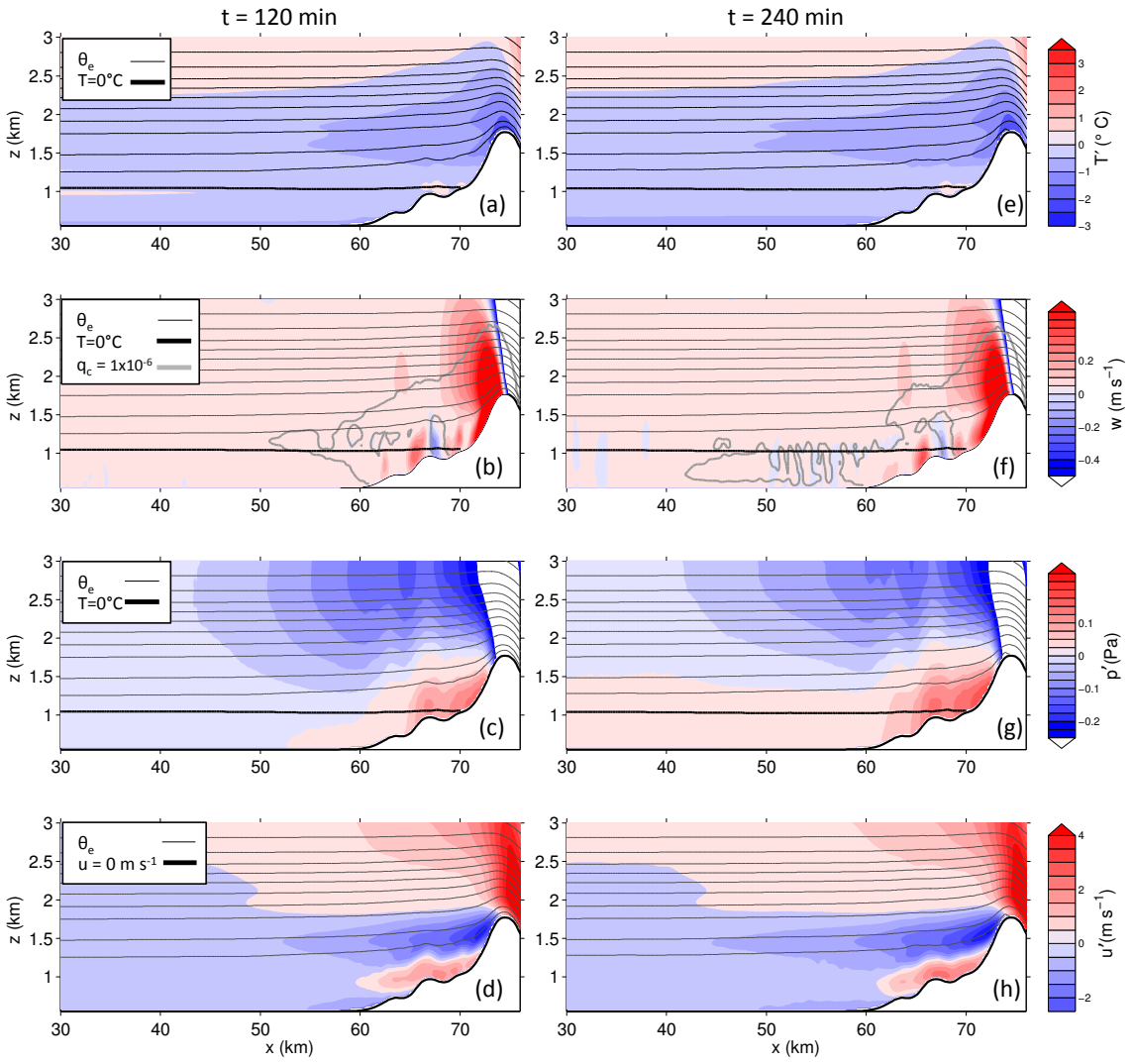

Figure 9: As in Fig. 8, but showing perturbation fields from the no temperature feedbacks from melting snow simulation.

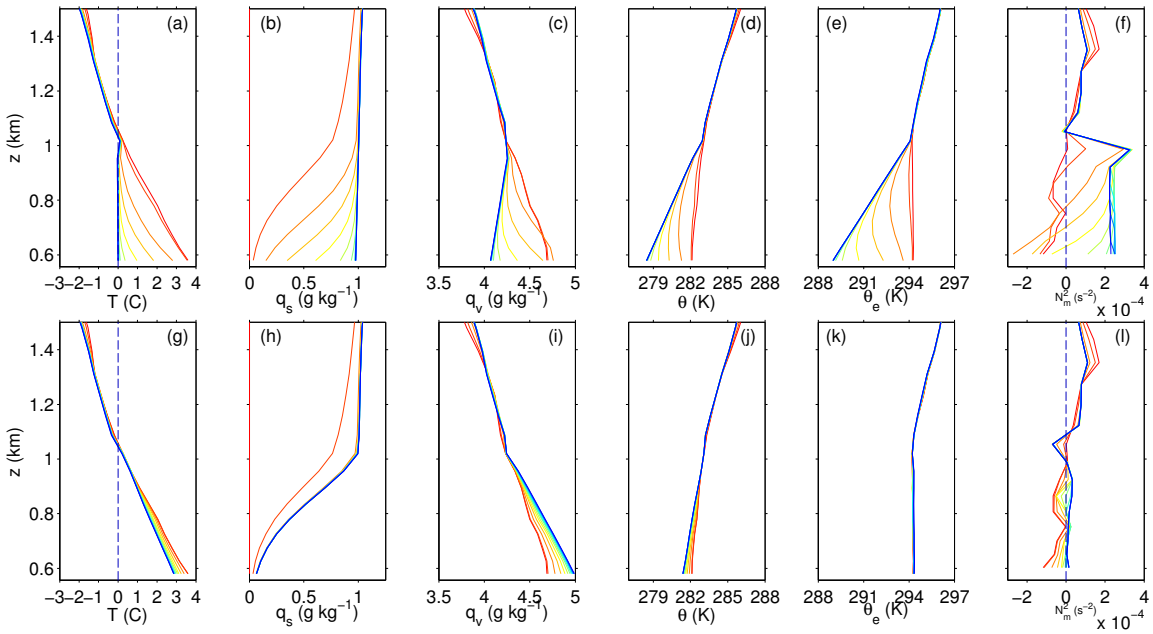

Figure 10: Lower atmospheric profiles taken from upwind boundary. Profiles are plotted every 10 min from t = 0-240 min. Profiles from t=0 are red and successive profilers progress towards blue. (a)-(f) shows results from the control simulation. (g)-(l) show results from the no temperature feedbacks from melting snow simulation.

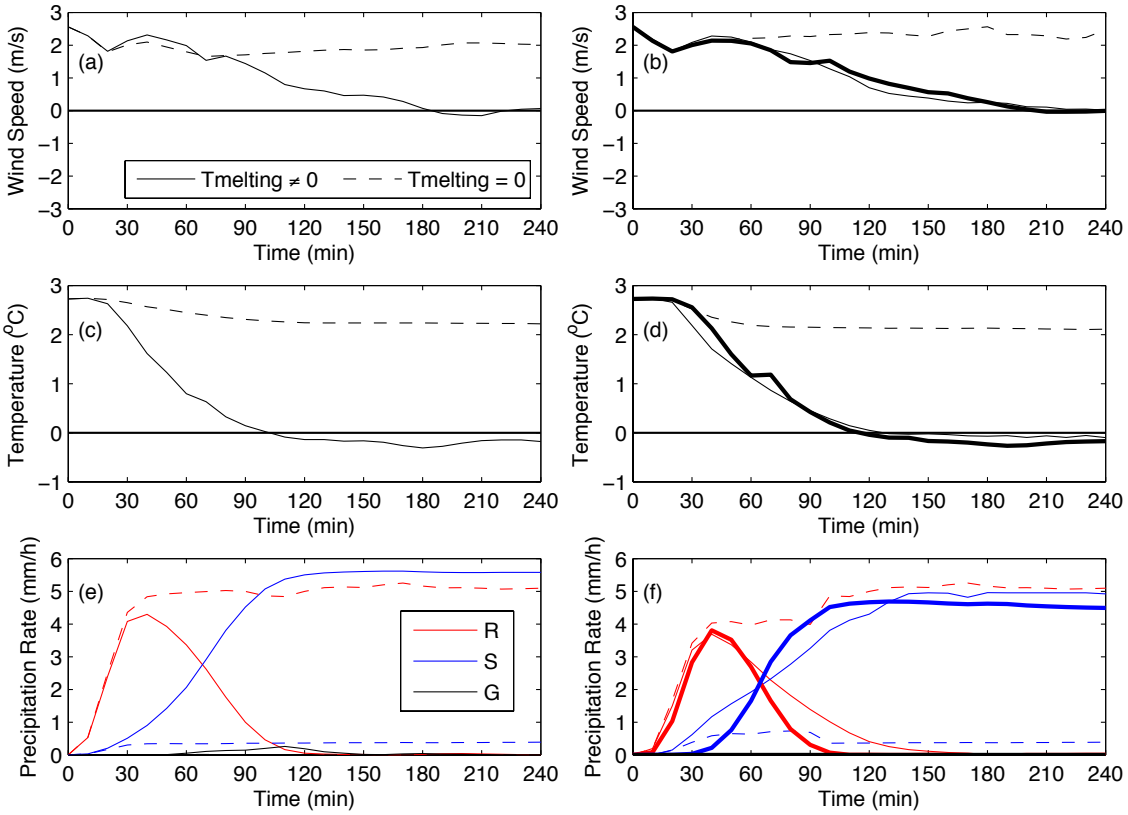

Figure 11: The comparison of the surface (a) and (b) wind speed, (c) and (d) temperature as well as (e) and (f) precipitation rates of rain(R), snow (S) and graupel (G) at the base of the mountain (VVO). The results are obtained using the MY2 scheme (left column). The left columns are the results from the THOM microphysics scheme and the GERBIN microphysics scheme (bold lines). The simulations with full microphysical processes (Tmelting $\neq$ 0) and with suppressing the effect of cooling from melting snow (Tmelting = 0) are shown for MY and THOM but only the (Tmelting $\neq$ 0) for the GERBIN.

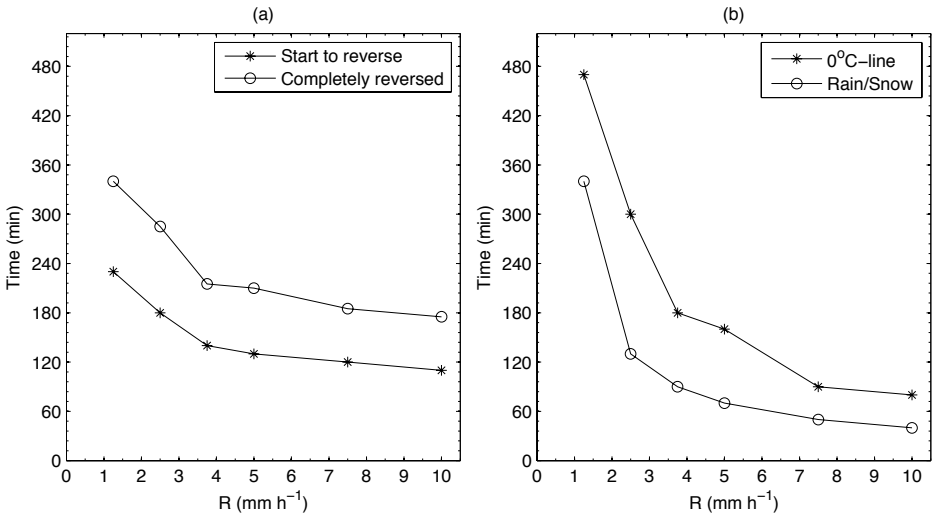

Figure 12: (a) The time needed for the valley flow field to start changing direction (Start to reverse) and to have changed direction throughout the depth of the melting layer at t = 0 (Completely Reversed) varying with the initial snow field aloft. (b) Time associated with the 0°C line and the 50/50 rain/snow to reach the base of the mountain.

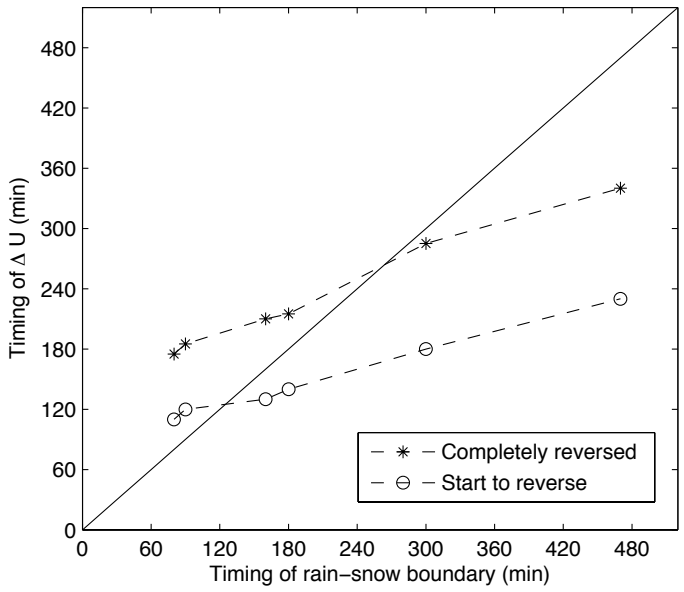

Figure 13: The relationship between the evolution of the valley flow field and the 0°C line reaching the base of the mountain. The dashed-line-circle is associated with the time needed for the valley flow field to start changing direction and the dashed-line-star is the time needed for the valley flow field to change direction throughout the depth of the melting layer at $t = 0$.